
CHAPTER 2

EXPERIMENTAL SECTION

CHAPTER-2

EXPERIMENTAL

2.1 Materials

2.1.1 Composition and dimensions of used Mild steel sample

The mild steel (MS) strip of 2 cm x 2.5 cm x 0.025 was used for weight loss and 8 cm x 1 cm x 0.025 cm dimensions was used for electrochemical study. The composition of MS is given as:

C	P	Si	Mn	Cr	Cu	Al	Ni	Fe
0.17%	0.46%	0.026%	0.050%	0.012%	0.135%	0.023%	0.05%	Balance

2.1.2 Test solution

The 1 M HCl test solution was prepared by diluting analytical grade 37% HCl with double distilled water.

2.1.3 Inhibitors

Twelve compounds were synthesized in the laboratory by the previously reported methods, characterised and evaluated as corrosion inhibitors for MS in 1 M HCl. These inhibitors are divided into four sections as given below:

A. Pyrano-pyrazoles(EPPs)

- a) Ethyl 6-amino-3-methyl-4-(p-tolyl) 2,4-dihydropyrano [2,3,C] pyrazole-5-carboxylate (EPP-1),
- b) Ethyl 6-amino-3-methyl-4(phenyl)-2,4dihydropyrano [2,3,C] pyrazole-5- carboxylate (EPP-2),
- c) Ethyl 6-amino-3methyl-4-(3-nitrophenyl) 2,4-dihydropyrano [2,3,C] pyrazole-5-carboxylate (EPP-3)

B. Schiff base derived from 2,6 diamino-pyridine(DAPs)

- a) N2, N6- bis(4-methylbenzylidene)pyridine-2,6-diamine (DAP-1),
- b) N2, N6-dibenzylidenepyridine- 2,6-diamine (DAP-2),
- c) N2, N6- bis(4-nitrobenzylidene)pyridine-2,6-diamine (DAP-3)

C. Imidazoles(IMs)

- a) 2-(3-methoxyphenyl)-4,5-diphenyl-1H-imidazole (IM-1)
- b) 2,4,5-triphenyl-1H-imidazole (IM-2)
- c) 2-(3-nitrophenyl)-4,5-diphenyl-1H-imidazole (IM-3)

D. Pyrazolo-pyridine(PPs)

- a) (4-(4-methoxyphenyl)3,5-dimethyl-1,4,7,8-tetrahydrodipyrzoloypyridine) (PP-1)
- b) 3,5dimethyl-4-phenyl-1,4,7,8-tetrahydrodipyrzoloypyridine (PP-2)
- c) (3,5-dimethyl-4-(3-nitrophenyl)-1,4,7,8-tetrahydrodipyrzoloypyridine) (PP-3)

2.2 Synthesis of inhibitors

(A) Synthesis of Pyrano-pyrazoles (EPPs) [Samy A. El-Assaly. (2011)]

To a stirred aqueous mixture of hydrazine hydrate 96% (2 mmol) and ethyl acetoacetate (2 mmol), aromatic aldehyde (2 mmol), ethyl cyanoacetate (2 mmol) and triethylamine (1ml) were added successively at room temperature with vigorous stirring for 20-30 min. The precipitated solid was filtered, washed with water and the product obtained was purified by recrystallization from ethanol.

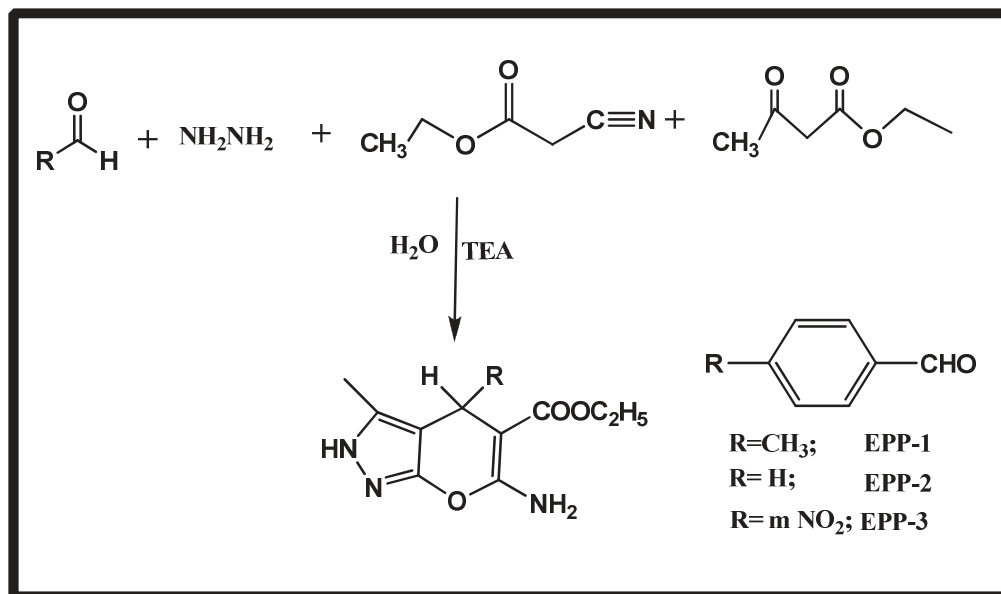
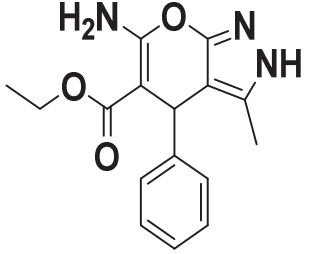
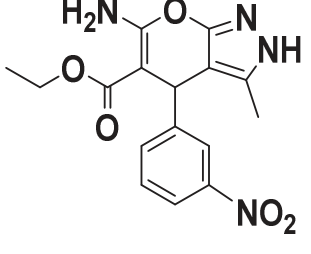


Figure 2.1.1 Synthesis of Pyrano-pyrazoles derivatives.

Table 2.1.1 The molecular structure and IUPAC name of synthesized Pyrano-pyrazoles

IUPAC Name	Molecular Structure	Analytical Data
(Ethyl 6-amino-3-methyl-4-(p-tolyl) 2,4-dihydropyrano[2,3,C]pyrazole-5-carboxylate) (EPP-1)		Off white crystalline powder; m.p= 190-200°C; ¹ H NMR (500 MHz, DMSO-d ₆):δ (ppm)=2.20 (CH ₃), 4.19 (CH ₂), 4.75 (CH), 6.83 (NH ₂) 7.08–7.42 (Ar-H), 11.82 (NH) ¹³ C NMR (DMSO-d ₆):δ (ppm)=13.44, 21.88,34.82,60.84,79.12,114.2 2,124.28,129.26,135.24,140.4 4,160.12,164.54,170.82

<p>Ethyl (6-amino-3-methyl-4(phenyl)-2,4-dihydropyrano[2,3,C]pyrazole-5-carboxylate) (EPP-2)</p>		<p>Off white crystalline powder; m.p= 273°C;</p> <p>¹H NMR (500 MHz, DMSO-d₆):δ (ppm)= 1.96 (CH₃), 4.21 (CH₂), 4.96 (CH), 6.89 (NH₂), 7.21–7.45 (Ar-H), 12.06 (NH)</p> <p>¹³C NMR (DMSO-d₆):δ (ppm)= 13.82, 35.60, 62.02,79.20, 113.24,126.01, 129.42, 139.72, 143.18, 159.28, 163.88, 169.92</p>
<p>(Ethyl 6-amino-3methyl-4-(3-nitrophenyl) 2,4-dihydropyrano[2,3,C] pyrazole-5-carboxylate) (EPP-3)</p>		<p>Pale yellow crystalline powder ; m.p= 260-263°C; ¹H NMR (500 MHz, DMSO-d₆):δ (ppm)=1.93 (CH₃), 4.31 (CH₂), 4.71(CH), 6.83(NH₂) 7.45– 8.32 (Ar-H), 11.95 (NH)</p> <p>¹³C NMR (DMSO-d₆):δ (ppm)= 13.88,33.62, 61.54, 79.22, 113.80, 121.25, 133.10, 140.24, 147.82, 160.12, 164.28, 170.12</p>

(B) Synthesis of pyridine based Schiff bases derivatives [Murad (2014)]

A mixture of 2, 6-diaminopyridine (1.0mmol) and various substituted aromatic aldehydes were taken in round bottom flask. On addition of 50ml of ethanol in to the reaction mixture and refluxed this mixture approximately 3-5h. After it obtained solid mass was recrystallized from ethanol. The chemicals used for this synthesis were obtained from Merck and SD Fine, India.

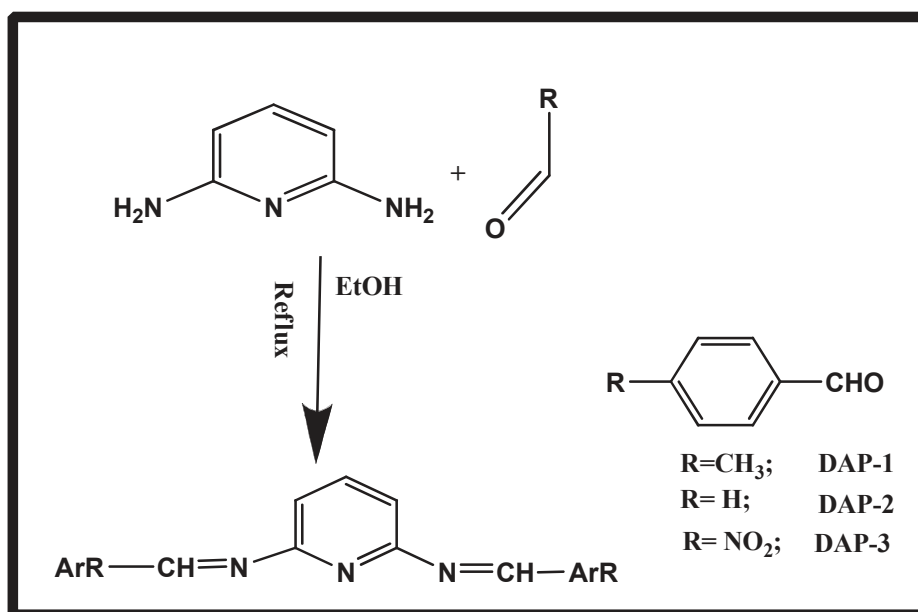
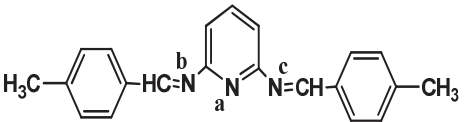
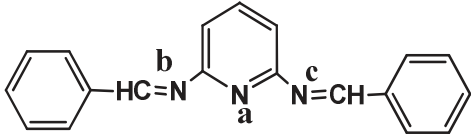
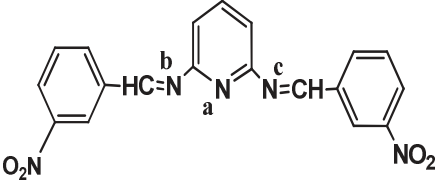
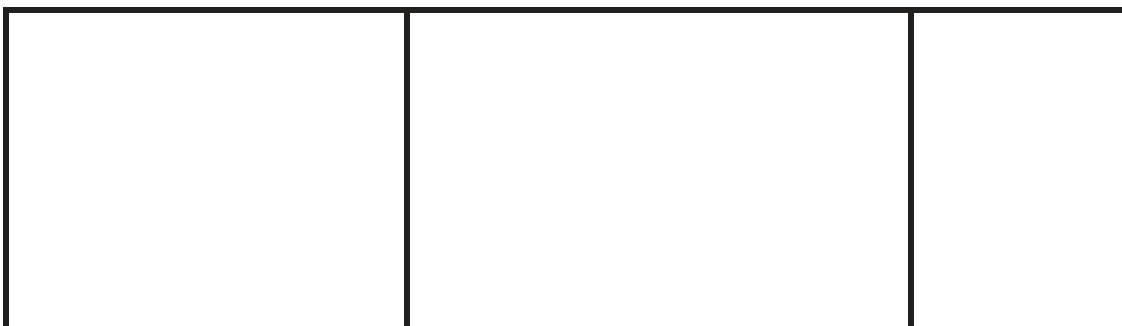


Figure 2.1.2 Synthesis of pyridine based Schiff bases derivatives.

Table 2.1.2 The molecular structure and IUPAC name of synthesized pyridine based Schiff bases derivatives.

Inhibitors	Molecular Structures	Analytical Data
N2, N6-bis(4-methylbenzylidene)pyridine-2,6-diamine (DAP-1)		<p>C₂₁H₁₉N₃, 313.40, 3030(Ar-CH), 1620(C=N), 1570(C=C), 2880 aliphatic (C-H) 1H NMR (500 MHz, DMSO) 1H NMR (DMSO-d₆):7.91-8.03 (3 H;CH Pyridine), 7.11-7.56 (m,10H, CH benzene, 5.27(2H,2N-CH-C) 2.7-3.2 (6H,CH₃)</p>
N2, N6-dibenzylidenepyridine- 2, 6-diamine (DAP-2),		<p>C₁₉H₁₅N₃, 285.13, 3021(Ar-CH), 1623(C=N), 1580(C=C)</p>

		<p>¹H NMR (500 MHz, DMSO)</p> <p>¹H NMR (DMSO-d₆):7.88-8.16 (m,3 H;CH Pyridine),</p> <p>7.11-7.56 (m,10H, CH benzene,</p> <p>5.66(2H,2N-CH-C)</p>
<p>N², N⁶-bis(4-nitrobenzylidene)pyridine-2,6-diamine (DAP-3)</p>		<p>C₁₉H₁₃N₅O₄,</p> <p>375.10,</p> <p>3015(Ar-CH),</p> <p>1630(C=N),</p> <p>1565(C=C)</p> <p>¹H NMR (500 MHz, DMSO)</p> <p>¹H NMR (DMSO-d₆):7.87-8.06 (3 H;CH Pyridine),</p> <p>7.02-7.46 (10H, CH benzene,</p> <p>5.26(2H,2N-CH-C)</p>



(C) Synthesis of Imidazole derivatives [Nemati *et al.* (2013)]

A mixture of benzyl (1.0mmol), substituted aldehyde (1.1mmol) and ammonium acetate (2.0mmol) were taken in the RB flask. Now add 5-6 ml of glycerol and stirred the mixture at 90°C. After 3-5hr the obtained reaction mixture was poured in the water. The precipitated solid was filtered, washed with water and the obtained product was purified and recrystallization from ethanol.

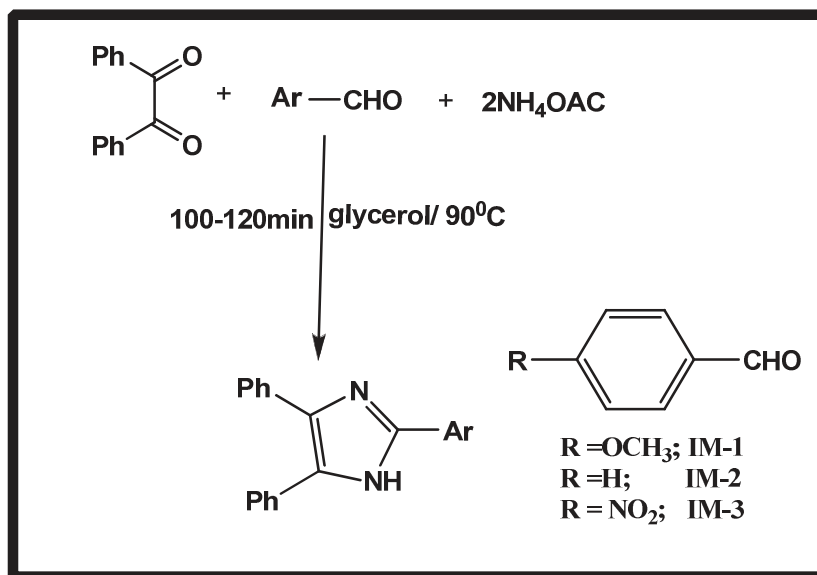
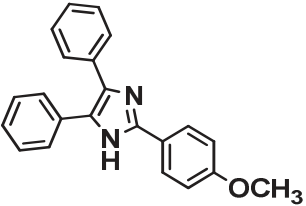
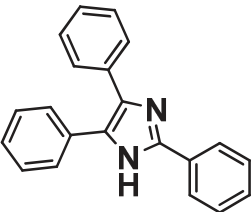
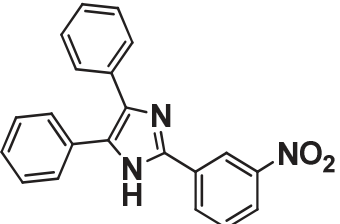


Figure 2.1.3 Synthesis of Imidazole derivatives.

Table 2.1.3 The molecular structure and IUPAC name of synthesized Imidazole derivatives.

Inhibitors	Molecular Structures	
2-(3-methoxyphenyl)-4,5-diphenyl-1H-imidazole (IM-1)		$C_{22}H_{18}N_2O$; 326.14 ; Off white crystalline powder; m.p= 190°C
2,4,5-triphenyl-1H-imidazole		$C_{21}H_{16}N_2$; 296.13; Off white crystalline powder; m.p= 223°C;
2-(3-nitrophenyl)-4,5-diphenyl-1H-imidazole (IM-3)		$C_{21}H_{15}N_3O_2$; 341.12, Pale yellow crystalline powder ; m.p= 321°C;

(D) Synthesis of Pyrazolo-pyridine (PPs) derivatives [Dabiri *et al.* (2014)]

A mixture of hydrazine hydrate (2.0mmol), β -dicarbonyl compound (2.1 mmol), appropriate substituted aldehydes (1.0mmol) and (4.0mmol) of ammonium acetate in 10 mL EtOH was introduced in a heavy walled beaker. The beaker was attached to a 12 mm tip diameter probe, and the reaction mixture was sonicated for the specified period at 50% power of the

processor and in a 5 s pulse mode until a solid product separates out. Completion of the reaction was monitored by TLC using n-hexane:ethyl acetate (7:3) as the eluent. All the reactions were invariably completed in 30-40 min. The molecular structure, analytical data and abbreviations of the inhibitors are given Table 2.1.4. Ultrasound irradiation was provided by an ultrasonic processor probe (Processor Sonics and material inc. VCX75 S/N 79348AE-03-14Ultrasonics with power input 230 V, 50 Hz, 8 Amps, and power variac 0–230 V and 8 Amps) operating at 20 kHz and 750W with 6 mm/12 mm tip diameter probes. Earlier these compounds were synthesized by chemical method under reflux condition in 4-8 hr

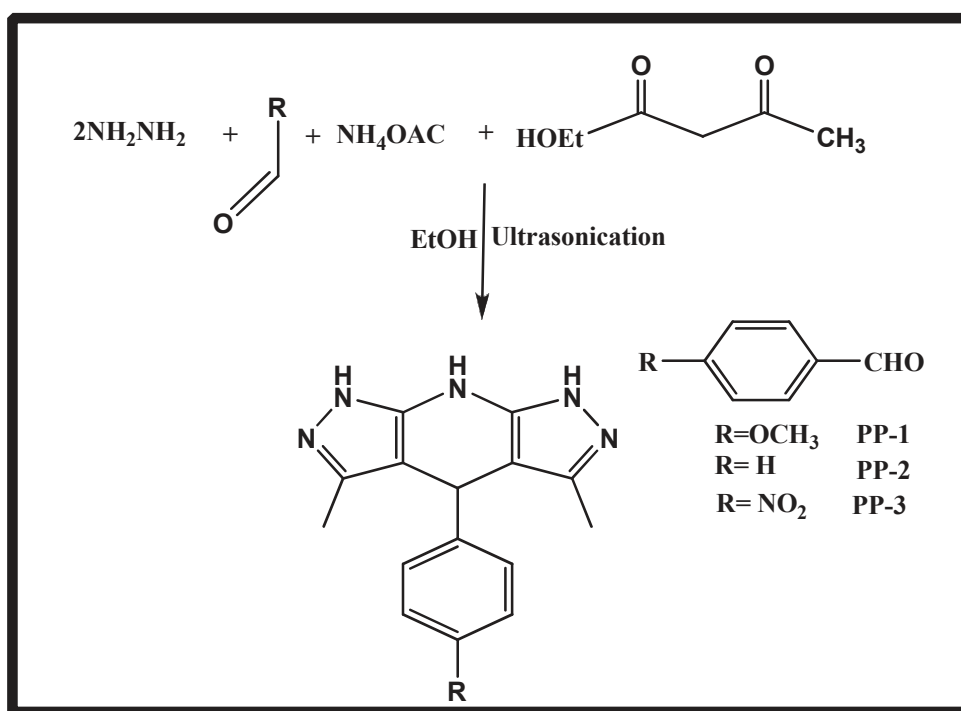
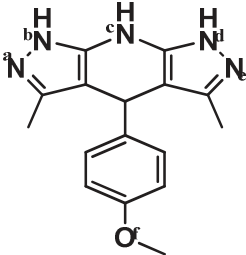
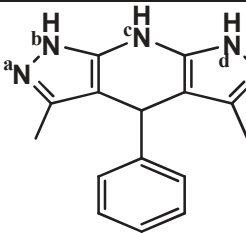
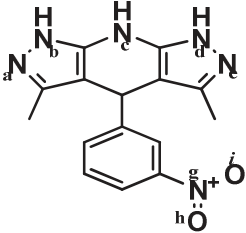


Figure 2.1.4 Synthesis of Pyrazolo-pyridine (PPs) derivatives.

Table 2.1.4 The molecular structure and IUPAC name of synthesized Pyrazolo-pyridine derivatives.

IUPAC Name	Molecular Structure	Analytical Data
(4-(4-methoxyphenyl) 3,5-dimethyl-1,4,7,8-tetrahydrodipyrzolo pyridine) (PP-1)		White crystalline powder; m.p= 321-323°C; ¹ H NMR (500 MHz, DMSO) δ (ppm): 1.48, 3.77, 4.38, 4.63, 6.87-7.32, 10.93, 11.96
3,5dimethyl-4-phenyl-1,4,7,8-tetra hydro dipyrzolo pyridine (PP-2)		White crystalline powder; m.p= 271-273oC; 1H NMR (500 MHz, DMSO) δ (ppm): 1.49, 4.65, 4.41, 7.12-7.56, 6.87-7.32, 10.96, 11.99
(3,5-dimethyl-4-(3-nitrophenyl)-1,4,7,8-tetrahydrodipyrzolo pyridine) (PP-3)		Pale yellow crystalline powder ; m.p= 271-273oC; 1H NMR (500 MHz, DMSO) δ (pp): 1.93, 4.0, 5.34, 7.53- 8.16,

		7.59 12.62
--	--	------------

2.3 Equipments and techniques used

2.3.1. Characterization of the Synthesized Compounds

(i) Determination of melting point

Melting points of the synthesized compounds were determined in open capillaries using Reichert ThermoVar apparatus.

(ii) Spectroscopic characterization

Synthesized compounds were characterized using Infra-red (IR) and ¹H NMR spectroscopic methods. The IR spectra were recorded using Perkin Elmer (Spectrum100) Fourier transform (FT-IR) spectrophotometer whereas the ¹H NMR spectra at 500 MHz was recorded using the JEOL AL 300 FT-NMR in DMSO-D₆ in which Tetramethylsilane (TMS) was used as internal standard.

2.3.2. Determination of corrosion rate and other related parameters

2.3.2.1 Weight loss method for determination of corrosion rate

Weight loss experiments were performed using MS coupons having following dimension 2.5 cm × 2.0 cm × 0.025 cm. These MS samples were abraded by using emery paper (600-1200 grade) then washed with double distilled water and finally dried. The surface area of the MS samples was measured by the following equation [ASTM (1990)],

$$A = 2(lb + lt + bt - \pi r^2 + \pi r t) \quad (2.1)$$

where, l represent length, b width, t thickness of the sample in cm and r is the radius of the mounting hole.

The weight loss experiment was conducted by correctly weighed MS samples and immerses them with the help of thread in a 100 ml conical flask in absence and presence of used inhibitors for 3 h. The experiment was performed in varying concentration and solution temperature. The weight loss experiments were performed in triplicate to ensure the reproducibility for observations. After, the completion time, these MS samples were taken out washed with water then dried and weighed. By calculating the difference in weight loss before and after immersion time, following parameters can be calculated such as corrosion rate, C_R inhibition efficiency, $\eta\%$ and surface coverage, θ using following equations [ASTM (1987)],

$$C_R = \frac{W}{dAt} \quad (2.2)$$

$$\eta\% = \frac{C_R - \text{inh}C_R}{C_R} \times 100 \quad (2.3)$$

$$\theta = \frac{C_R - C_{R(i)}}{C_R} \quad (2.4)$$

where W is the average weight loss, a is total surface area of MS specimen, t is the immersion time (3 h) and D is the density of MS in (gcm^{-3}). In equation (2.3) C_R and $C_{R(i)}$ is the corrosion rates of MS in the absence and presence of the inhibitors respectively...

2.3.2.2 Electrochemical measurements

The electrochemical experiments: Electrochemical impedance spectroscopy (EIS) and Potentiodynamic polarization were conducted by using a three-electrode cell system

connected to the Potentiostat/Galvanostat G300-45050 (Gamry Instruments Inc., USA). Gamry Echem Analyst 5.50 software package was used for data analyses, and fitting [ASTM (1991)]. In this three-cell system the MS strips of 8 cm x 1 cm x 0.025 cm dimension with exposed area of 1 cm² is used as working electrode. The graphite and saturated calomel electrodes (SCE) are used as auxiliary and reference electrodes correspondingly. All experiments were carried out at 308 K. The electrochemical experiments were performed after immersing the MS strips for 30 min in the respective testing solutions.

2.3.2.2.1 Electrochemical impedance spectroscopy:

EIS measurements were carried out in a frequency range from 100 kHz to 0.01 Hz, with amplitude of 10 mV AC signal using three electrode systems. The impedance parameters like R_{ct} , C_{dl} were analyzed by using equivalent circuit model for data fitting containing R_s (solution resistance), CPE (constant-phase element) parallel to the R_{ct} (charge-transfer resistance). The CPE is used in the model for accurately determining the depressed capacitive semi-circle Nyquist loops. This appearance of the loops is attributed due to the surface roughness, frequency dispersion, relaxation and porous surface of MS. The impedance function of the CPE is expressed by the equation [Ahamad and Quraishi (2010)],

$$Z_{CPE} = Y^{-1}(j\omega)^{-n} \quad (2.5)$$

where Y is the amplitude of CPE, j is the square root of -1, ω is angular frequency and n is the phase shift.

The R_{ct} was obtained by calculating the difference in impedance at lower and higher frequencies which is attributed due to the resistance developed between outer Helmholtz planes of metal surface. The corrosion inhibition efficiency ($\eta\%$) and corresponding double layer capacitance (C_{dl}) was calculated by the following equations [Ahamad *et al.* (2010)],

$$\eta\% = \left(\frac{R_{p(i)} - R_p}{R_{p(i)}} \right) \times 100 \quad (2.6)$$

where R_{ct} and $R_{ct(i)}$ are the values of charge transfer resistance in the absence and presence of inhibitors respectively.

$$C_{dl} = \frac{Y^o \omega^{n-1}}{\sin(n(\pi / 2))} \quad (2.7)$$

where, ω is angular frequency and n is the phase shift, which depicts the heterogeneity or surface roughness for MS.

2.3.2.2.2 Potentiodynamic polarization:

The Potentiodynamic polarization analysis were performed by sweeping the electrode potential range from -0.25 V to $+0.25$ V versus open circuit potential at a scan rate of 1.0 mVs⁻¹ scan rate. The parameters like corrosion potential, E_{corr} corrosion current density, i_{corr} were calculated after analysis of the obtained data. The inhibition efficiencies were calculated from i_{corr} values using the following equation [Shukla and Quraishi (2009)],

$$\eta\% = \frac{i_{corr} - i_{corr(inh)}}{i_{corr}} \times 100 \quad (2.8)$$

where, i_{corr} and $i_{corr(inh)}$ shows the corrosion current densities in the absence and presence of inhibitors respectively, in 1 M HCl.

2.4 Thermodynamic parameters

2.4.1 Activation energy: The effect of temperature on activation energy for MS is calculated by using Arrhenius equation [Singh and Quraishi (2010)],

$$\ln(C_r) = \frac{-E_a}{RT} + A \quad (2.9)$$

where, E_a is the activation energy for corrosion of MS, R is the gas constant, A the Arrhenius pre-exponential factor and T is the absolute temperature. A plot between the corrosion rate and temperature ($\log C_r$ vs $1000/T$) gives a straight line. The activation energy in absence and presence of inhibitor is determined by the slope obtained from the plot.

2.4.2 Free energy of adsorption: The interaction between inhibitor molecules and MS surface can be better understood by adsorption isotherm. The adsorption of inhibitor molecules on the corroding MS surface not attains the complete equilibrium. When retardation in corrosion rate occurs in presence of inhibitor then a quasi equilibrium state occurs through the adsorption process. The nature of quasi equilibrium adsorption of inhibitors can be investigated using appropriate adsorption isotherm. Different adsorption isotherms including Langmuir, Temkin and Freundlich isotherms used to fit the observed experimental results are given as [Yadav and Quraishi (2012) (a)],

Temkin isotherm

$$\exp(f \cdot \theta) = K_{ads} \cdot C \quad (2.10)$$

Freundlich isotherm

$$\theta = K_{ads} \cdot C \quad (2.11)$$

Langmuir isotherm

$$(\theta/1-\theta) = K_{ads} \cdot C \quad (2.12)$$

where, K_{ads} designates the equilibrium constant for adsorption process, C is the concentration of inhibitor and f is energetic inhomogeneities. The free energy of adsorption can be calculate by the following equation [Yadav and Quraishi (2012) (a)],

$$\Delta G_{ads} = -RT \ln(55.5K_{ads}) \quad (2.13)$$

where, T represent the absolute temperature and R stands for the gas constant. In this equation 55.5 is the concentration of water in solution in mol L⁻¹.

2.5 Scanning electron microscopy (SEM)

Surface morphology of MS in absence and presence of inhibitors is analysed by SEM. The 3 h immersed without and with inhibitor of MS samples having following dimensions 2.5 cm × 2.0 cm × 0.025 cm was cut into 1 cm² size for surface analysis. These prepared samples were analysed by using SEM model Supra 40, Carl Zeiss, Germany at 500 x magnifications.

2.6 Atomic force microscopy (AFM)

AFM is another method for surface analysis. The MS surface in absence and presence of inhibitor was analysed by using NT-MDT multimode, Russia, controlled by a solver scanning probe microscope controller.

2.7 Quantum chemical calculations

The Quantum chemical measurements were performed using the density functional theory (DFT) for the studied compounds. The Becke three-parameter hybrid functional along with Lee-Yang-Paar correlation functional (B3LYP) used in DFT [Becke (1993)], [Becke (1998)], [Lee *et al.* (1998)]. For all the calculations, the basis set 6-31+G (d, p) was selected. This computational study was carried out by using the Gaussian 09, software (Revision D.01) for Windows [Frisch *et al.* (2009)]. The effects of water on the geometry and electronic parameters were modelled using the integral equation formalism polarisable continuum model (IEFPCM) implemented in Gaussian 09. The studied compounds were first optimized and confirmed to correspond in its true energy minima by the absence of the imaginary frequency in the computed vibrational frequencies. The obtained quantum chemical

parameters were explicated on the basis of their electronic parameters and also the most stable state of molecules conformation. The Frontier molecular orbitals (FMO), that is, the highest occupied molecular orbital energy (E_{HOMO}) and the lowest unoccupied molecular energy (E_{LUMO}) were calculated. Likewise the energy gap (ΔE), global electronegativity (χ), and fraction of electron moved from inhibitor to metal atom were calculated by the following equations [Martinez (2003)], [Olasunkanmi *et al.* (2015)], [Musa et al (2012)], [Zhao et al (2015)], [Hassan et al (2005)], [Zhao et al(2014)]

$$\Delta E = E_{LUMO} - E_{HOMO} \quad (2.14)$$

$$\chi = -\frac{1}{2}(E_{LUMO} + E_{HOMO}) \quad (2.15)$$

$$\Delta N = \frac{\chi_{Fe} - \chi_{inh}}{2(\eta_{Fe} + \eta_{inh})} \quad (2.16)$$

where χ_{Fe} and η_{inh} respectively represent the electronegativity and hardness of iron and inhibitor.

The electronegativity 7 eV/mol value is used for χ_{Fe} , and hardness for η_{Fe} was taken as 0 eV/mol for bulk Fe atom based on the Pearson's electronegativity scale [Pearson (1988)].

The global hardness (η) and softness (σ) are calculated according to following equations,

$$\eta = \frac{E_{HOMO} - E_{LUMO}}{2} \quad (2.17)$$

$$\sigma = \frac{1}{\eta} \quad (2.18)$$

The calculated parameters like global hardness (η) and softness (σ) represent the reactivity of the molecule towards bond formation with metal [Abd El-Lateef (2015)].

The Fukui functions were calculated using the UCA-FUKUI v 1.0 software. Via Finite Difference (FD) method (Márquez et al) with the use of the output file from Gaussian 09. The Fukui function (f_k) is the first derivative of the electronic density with respect to the number of electrons N , in a constant external potential and written as follows: The Fukui functions f_k^+ and f_k^- represent the local reactivity indices. By these parameters the susceptibility of active atomic sites of inhibitor molecules can be known for the electrophilic and nucleophilic attacks [Gomez *et al.* (2006)], [Yan *et al.* (2013)]. The approach of the atom condensed Fukui functions with using Mullikan population analysis (MPA) and the finite difference (FD) approximations was introduced by Yang and Mortier [Yang and Mortier (1986)], and recently employed in another study were calculated as,

$$f_k^+ = \rho_{k(N+1)}(r) - \rho_{k(N)}(r) \quad (2.19)$$

$$f_k^- = \rho_{k(N)}(r) - \rho_{k(N-1)}(r) \quad (2.20)$$

$$f_k^0 = \frac{q_k(N+1) - q_k(N-1)}{2} \quad (2.21)$$

where f_k^+ and f_k^- stand for the electrophilic and nucleophilic Fukui indices, that is condensed with atom the k and $\rho_{k(N+1)}, \rho_{k(N)}, \rho_{k(N-1)}$ represent the electron densities of the (N+1)-, (N)- and (N-1)- electron systems accordingly, approximated based on Mullikan gross charges.

2.8 Monte Carlo simulations

Monte Carlo simulations were carried out to model the mode of adsorption of the studied inhibitor molecules on iron surface. The adsorption locator code implemented in the Material Studio 7.0 software from Biovia-Accelrys Inc. USA was adopted to compute the adsorption energy of the interaction between the inhibitor molecules and clean iron surface.

The universal force field (UFF) was used in the entire simulation process for the optimization of the structures. Fe (110) crystal surface was selected for this simulation and to represent MS because it is the most stable surface. The Fe (110) surface was cleaved with a thickness of 5 Å. Then this cleaved plane was just enlarged to a (10 × 10) super cell. After that a vacuum slab of 30 Å thicknesses was built over the Fe (110) plane. The studied inhibitor molecules were used for the simulations in each case. The simulated annealing procedure adopted in this study uses the Monte Carlo method to determine the adsorption energy of the adsorbate substrate. During the simulated annealing, the adsorbate is heated and then cooled very slowly so that conformational changes taking place will lead to a local minimum being located. The process was repeated several times until very closely related, low energy conformations were obtained. Extensive literature about the Monte Carlo simulation can be found elsewhere [Saha *et al* (2015**a**)], [Zhang *et al.* (2016)], [Musa *et al* (2011)].